Research Article

Raja Saad Alruwais*

Investigating dye adsorption: The role of surface-modified montmorillonite nanoclay in kinetics, isotherms, and thermodynamics

https://doi.org/10.1515/chem-2024-0116
received August 26, 2024; accepted November 4, 2024

Abstract: The study presents a straightforward, eco-friendly method for removing toxic dyes, such as methylene blue (MB) and acid red (AR), from aqueous solutions through solid-phase extraction using adsorption on surface-modified montmorillonite nanoclay. The nanoclay, containing 25–30 wt% methyl dihydroxyethyl hydrogenated tallow ammonium (MM-MDH nanoclay), functions as the environmentally benign adsorbent. The physical properties of MM-MDH nanoclay were characterized utilizing scanning electron microscopy, transmission electron microscopy, X-ray diffraction, Fourier transform infrared spectroscopy, and surface area analysis. Optimal conditions for dye removal, including solution pH, nanoclay dosage, contact time, solution temperature, and ionic strength, were systematically investigated. Experimental results demonstrated that MM-MDH nanoclay effectively removed the majority of dyes within 90 min. Isotherm data indicated an adsorption capacity of 34.33 mg/g for AR dye and 20.19 mg/g for MB dye under optimal conditions. The adsorption process was analyzed kinetically and thermodynamically, revealing that the pseudo-second-order kinetic model accurately described the adsorption behavior. Thermodynamic analysis confirmed that the process was spontaneous and exothermic for AR dye and spontaneous and endothermic for MB dye. The effectiveness of MM-MDH nanoclay was further validated by removing dyes from three different real samples, demonstrating high performance in dye removal over four consecutive cycles.

Keywords: methylene blue, acid red, nanoclay, adsorption, kinetics, thermodynamic, isotherm

*** Corresponding author: Raja Saad Alruwais,** Department of Chemistry, Faculty of Science and Humanities, Shaqra University, P.O. Box 33, Dawadmi, 17452, Saudi Arabia, e-mail: ralruwais@su.edu.sa

1 Introduction

Water is an essential resource for life, supporting ecosystems, human health, and economic development. However, water contamination with toxic dyes from industrial effluents poses a significant threat to aquatic environments and public health. Methylene blue (MB), a cationic dye, is extensively used in industries such as textiles, paper, and plastics due to its vibrant color and chemical stability [1]. Similarly, acid red (AR), an anionic dye, is commonly used in textile dyeing, food processing, and cosmetics, contributing significantly to industrial wastewater [2]. Both dyes are known for their resistance to degradation, posing persistent environmental hazards due to their ability to inhibit aquatic photosynthesis and potentially cause toxic effects on marine life [3]. By focusing on these dyes, our study addresses contaminants that are not only prevalent in industrial effluents but also pose significant challenges in water treatment due to their chemical properties. This relevance ensures that the findings of our research have practical implications for improving industrial wastewater management and environmental conservation efforts. Numerous countries globally depend significantly on the textile industry for economic prosperity. Effluents from several industrial sectors such as textiles, dyeing, and leather processing often contain synthetic dyes. These effluents, characterized by their vivid coloration, significantly pollute water bodies. Currently, the market offers more than 10,000 types of dyes, each with unique chemical properties. Depending on their molecular ionic charge, these dyes are classified into three groups: anionic, cationic, and nonionic [4]. Dyes in aquatic environments can severely impact marine life by obstructing oxygen consumption and photosynthesis. Additionally, some dyes have the potential to be toxic or even carcinogenic [5–7]. Many dyes resist breakdown via hydrolysis due to their stability against light, oxidation, and aerobic processes. The presence of industrial dyes in the environment is problematic, as they and their byproducts can be carcinogenic and toxic. Addressing the pollution caused by synthetic organic dyes in wastewater has become increasingly

important. These dyes are particularly challenging to treat because they originate from synthetic materials, contain aromatic compounds, and do not readily biodegrade. To treat dyed wastewater, a variety of biological and physical/chemical approaches have been used. Photodegradation [8], coagulation/flocculation [9], oxidation/ozone [10], membrane separation [11], and adsorption [12] are some of these processes. Adsorption stands out as a crucial technique for extracting dyes from wastewater, among various chemical and physical methods successfully implemented. Currently, a significant challenge in sorption technologies involves identifying and deploying novel adsorbents capable of efficiently eliminating diverse pollutants from water-based environments [13,14]. Traditional methods of dye removal, including chemical precipitation, oxidation, and biological treatment, often fall short due to inefficiency, high cost, or secondary pollution issues. Therefore, there is an urgent need for simple, cost-effective, and eco-friendly methods to address this problem. This study explores the use of surface-modified montmorillonite nanoclay, specifically MM-MDH nanoclay, as an adsorbent for the removal of MB and AR dyes from aqueous solutions. The modification of montmorillonite with methyl dihydroxyethyl hydrogenated tallow ammonium enhances its adsorption capacity and environmental compatibility. MM-MDH nanoclay represents a significant advancement in the field of adsorbents due to its unique composition and enhanced performance characteristics. Unlike traditional adsorbents, MM-MDH nanoclay is modified with methyl dihydroxyethyl hydrogenated tallow ammonium, which notably increases its hydrophobicity and affinity for organic molecules. This modification allows MM-MDH nanoclay to achieve superior adsorption capacities, particularly for organic dyes like MB and AR 1, which are prevalent in industrial effluents. Furthermore, the nanoclay's surface modification enhances its selectivity, enabling it to target and remove specific contaminants more effectively than unmodified clay or other conventional adsorbents [15]. Additionally, MM-MDH nanoclay offers practical advantages in terms of environmental impact and cost-efficiency. It is more environmentally friendly, as it can be regenerated and reused in multiple cycles without significant loss of efficacy, reducing both waste and operational costs. These attributes make MM-MDH nanoclay a novel and advantageous solution in the treatment of polluted water, addressing both effectiveness in contaminant removal and sustainability concerns.

To effectively contextualize this study within the broader field of research, it is essential to examine previous studies that have articulated the environmental challenges posed by synthetic dyes in water systems. A review of the literature reveals a significant gap, while numerous methods have been explored for dye removal [16–18], few have effectively addressed the simultaneous demands of efficiency, cost-effectiveness, and environmental sustainability. Most existing studies focus on the immediate efficacy of removal techniques without considering long-term environmental impacts or feasibility in varied operational settings. This lack of comprehensive approaches to dye pollution has left a critical gap in sustainable water management practices. Our research addresses this gap by not only enhancing the adsorptive efficiency of montmorillonite nanoclay through surface modification but also emphasizing its reusability and minimal environmental footprint. By advancing a solution that upholds these core values, this study contributes uniquely to the ongoing dialogue on sustainable industrial practices and environmental stewardship.

This study aimed to evaluate the effectiveness of removing AR, an anionic dye, and MB, a cationic dye, from aqueous solutions and real water samples using MM-MDH nanoclay. This nanoclay contains 25–30 wt% methyl dihydroxyethyl hydrogenated tallow ammonium. The morphology of MM-MDH nanoclay was analyzed using various chemical and physical methods. Subsequently, different experimental conditions were tested and optimized for extracting AR and MB dyes from aqueous solutions using MM-MDH nanoclay. The kinetic and thermodynamic characteristics of the adsorption method were examined to gain insights into the desorption mechanism and the spontaneity of the process, aiming to enhance its efficiency. Finally, the study extended its findings to real-world scenarios by testing the effectiveness of MM-MDH nanoclay in removing AR and MB dyes from real water samples. This step was pivotal in confirming the practical utility of the nanoclay for environmental cleanup efforts, particularly showcasing its viability for purifying dye-polluted water sources. The findings underscored the substantial promise of MM-MDH nanoclay as an effective and eco-friendly adsorbent, offering considerable benefits for dye elimination across a spectrum of water treatment scenarios.

2 Materials and methods

2.1 Chemicals and materials

Nanoclay modified with methyl dihydroxyethyl hydrogenated tallow ammonium, identified as MM-MDH nanoclay (product number 682640) from Aldrich, was used in conjunction with AR 1 dye, MB dye, and hydrochloric acid (37%) purchased from Sigma Aldrich, USA. All employed chemicals and solvents were of reagent-grade quality and were used as received. Stock solutions of 500 mg/L were prepared for both dyes by dissolving 0.05 g of each in 100 mL of deionized water. These solutions were further diluted using deionized water to achieve concentrations ranging from 5 to 50 mg/L. Furthermore, a series of buffer

solutions from Britton-Robinson and an NaOH/HCl mixture ranging from pH 2 to 10, as well as 0.1 M hydrochloric acid, were used as the aquatic adsorption medium in this method.

2.2 Characterization techniques

The morphology of the MM-MDH nanoclay was characterized using a Quanta 600 FEG scanning electron microscope (SEM) and further analyzed with a JEOL JEM-1230 transmission electron microscope (TEM). The crystalline structure of the material was investigated through X-ray diffraction (XRD) using a Philips X-pert pro diffractometer. Fourier-transform infrared (FT-IR) spectroscopy was conducted with an RX1 FT-IR spectrometer, covering a range of 500–4,000 cm^{-1}. The specific surface area of the nanoclay was determined using a NOVA 3200e automatic gas sorption system.

2.3 Adsorption experiment

The study investigates the effectiveness of MM-MDH nanoclay as a solid-phase extractant for the removal of MB and AR dyes from aqueous solutions. A precisely measured 0.01 ± 0.002 g of MM-MDH nanoclay was introduced into a 25 mL aqueous solution of AR dye, with a concentration of 20 mg/L, in a conical flask. Hydrochloric acid (0.1 M) was used to adjust the solution's pH to 2. In another experiment, 0.0075 ± 0.002 g of the same nanoclay was added to a 25 mL solution of MB dye, with a concentration of 8 mg/L, and the pH was set at 8. Both mixtures were agitated for 120 min to reach equilibrium. Post agitation, the solutions were filtered, and the concentration of dyes left in the solution was quantified. The residual dye content was assessed using a UV–Vis spectrophotometer by comparing the absorbance values before and after adsorption at 530 nm for AR and 664 nm for MB [19]. Finally, the separation efficiency percentage (%E) is expressed by equation (1). Then, the quantity of dye adsorbed (q_t) on MM-MDH nanoclay is expressed by equation (2).

$$\%E = (C_o - C_t)/C_o \times 100, \quad (1)$$

$$q_t = ((C_o - C_t)V)/m, \quad (2)$$

where C_o is the concentration of initial dyes and C_t is the remaining concentration of dyes in the solution after shaking.

2.4 Practical investigation

To evaluate the effectiveness of MM-MDH nanoclay solid phase in the adsorption and removal of AR and MB dyes, water samples were collected from three distinct sources in Jeddah, Saudi Arabia. These included seawater from the Red Sea, wastewater from King Abdulaziz University's treatment facility, and tap water from the university's laboratories. The samples were filtered using a 0.45 µm membrane and stored at 5°C in dark conditions in Teflon containers. For experimental purposes, 25 mL of each sample was adjusted to pH 2 with 0.1 mol/L hydrochloric acid for AR dye and to pH 8 for MB dye. The samples were then agitated with MM-MDH nanoclay, and the dye concentrations were subsequently measured using spectrophotometry.

3 Results and discussion

Figure 1 shows the electronic spectra of AR dye and MB dye in the presence and absence of MM-MDH nanoclay. The figure depicts absorption spectra data, showing how the dyes' absorbance characteristics change when they interact with nanoclay. The data indicate a shift in the absorbance peak of the dyes when treated with MM-MDH nanoclay. For AR dye, one can infer that the initial absorption spectrum (without nanoclay) might display specific peak characteristics, which alter upon the addition of MM-MDH nanoclay due to interactions between the dye and the nanoclay particles. These interactions could include physical adsorption, where the dye molecules adhere to the surface of the nanoclay, or chemical interactions, leading to changes in the dye's electronic environment and thus its optical properties [20].

Similarly, for MB, the absorption characteristics before and after treatment with nanoclay demonstrate how effectively the nanoclay alters the dye's molecular environment. A reduction in peak intensity or a shift in the peak wavelength could indicate that the nanoclay is effective in binding or altering the dye, potentially by encapsulating it or changing its solubility and dispersion characteristics in the solution.

These spectral changes are critical as they indicate the potential of MM-MDH nanoclay in wastewater treatment applications. The ability of MM-MDH nanoclay to alter the absorption spectrum of toxic dyes implies that it could be used to remove or degrade these dyes from industrial effluents, thereby mitigating environmental pollution. From a scientific perspective, analyzing these spectra provides

insights into the interaction mechanisms at the molecular level between the nanoclay and the dye molecules. It also helps in optimizing the conditions for maximum removal efficiency, such as adjusting the nanoclay's concentration, contact time, and the pH of the solution. The initial spectrum for AR1 (20 mg/L) without MM-MDH nanoclay [Figure 1 (I)A] would show the dye's characteristic absorption peak, which the article mentions as occurring at 530 nm. This peak represents the wavelength at which AR1 absorbs most of the light, corresponding to its chromophoric groups' electronic transitions. After the addition of 10 mg of MM-MDH nanoclay, the spectrum [Figure 1 (I)B] shows a significant reduction in the peak at 530 nm. This decrease suggests that the nanoclay is interacting with the AR1 dye, possibly through adsorption or a chemical interaction that alters the dye's environment, thus reducing its ability to absorb light at this wavelength [21,22]. Similar to the AR, MB dye (8 mg/L) initially shows a prominent absorption peak at 664 nm [Figure 1 (II)A]. Upon the addition of 7.5 mg of MM-MDH nanoclay, the peak at 664 nm significantly diminishes [Figure 1 (II)B], which again indicates the adsorption or interaction of the dye with the nanoclay particles. This reduction in peak intensity underscores the effectiveness of MM-MDH nanoclay in removing dyes from water.

Surface modifications of montmorillonite nanoclay significantly impact the electronic environment of adsorbed dye molecules through a variety of interactions that alter their electronic properties [23]. When montmorillonite nanoclay is modified, typically with organic cations or other functional groups, it enhances its affinity for dye molecules through increased surface area and altered surface charge characteristics [24]. These modifications facilitate stronger electrostatic attractions, hydrogen bonding, and potential π–π stacking interactions between the nanoclay and the dye molecules. Such interactions can influence the electron density distributions within the dye molecules, leading to changes in their electronic transitions. This, in turn, affects the absorption spectra of the dyes, causing shifts in the wavelengths at which they absorb light. The modified surface of the nanoclay effectively creates a new microenvironment around the dye molecules that can stabilize or destabilize certain electronic states, thus directly impacting their optical properties and behavior under light exposure. This makes MM-MDH nanoclay a potent material for targeted dye adsorption and removal from aqueous solutions. Electrostatic interactions, hydrogen bonding, and π–π interactions significantly influence the spatial configuration and electron density of dye molecules when they are adsorbed on surfaces such as modified nanoclays [25]. Electrostatic interactions occur when there is a charge attraction between the negatively charged surface areas of the modified nanoclay and the oppositely charged sections of the dye molecules [20]. This can lead to a reorientation of the dye molecules to maximize the interaction with the clay surface, potentially altering the electronic distribution within the molecule. Hydrogen bonding, involving the sharing of a hydrogen atom between the dye and functional groups on the clay, can change the electronic environment by creating new electronic pathways and altering electron density distributions. This can lead to shifts in the absorption characteristics of the dye due to changes in their electronic states [26]. Lastly, π–π interactions, which occur between the aromatic rings of the dye molecules and similar structures on the clay surface, can stabilize specific spatial configurations

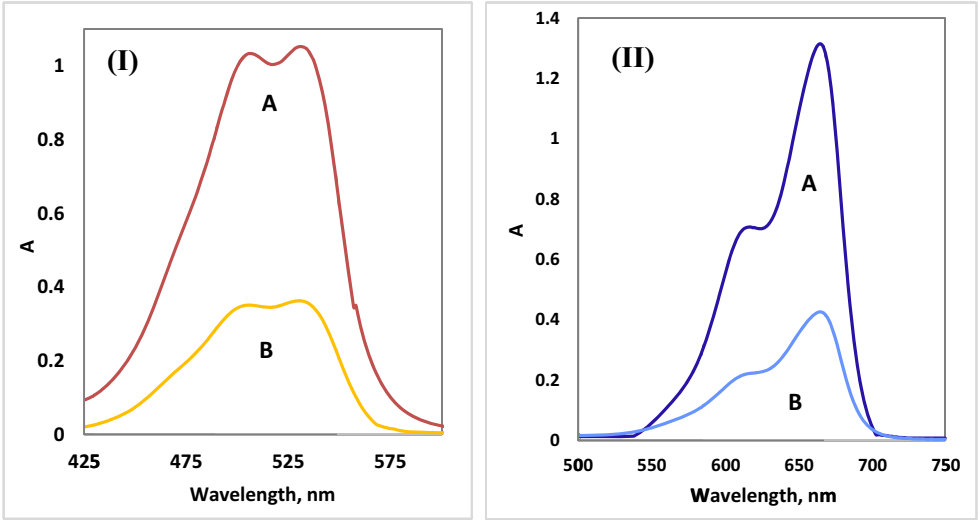

Figure 1: Absorption spectra analysis: Panel I (a): Baseline absorption spectrum of AR dye (concentration: 20 mg/L) without MM-MDH nanoclay. Panel I (b): Spectrum post interaction with 10 mg of MM-MDH nanoclay. Panel II (a): Initial absorption spectrum of MB dye (concentration: 8 mg/L) without MM-MDH nanoclay. Panel II (b): Spectrum after exposure to 7.5 mg of MM-MDH nanoclay.

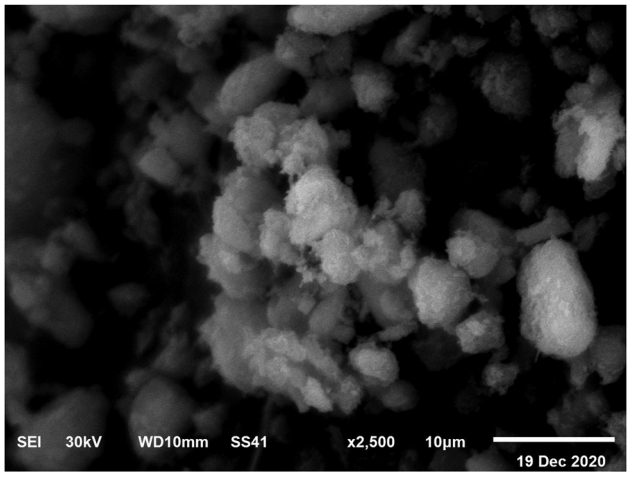

Figure 2: SEM images of MM-MDH nanoclay.

of the dyes. Such interactions can compress or extend the electron cloud of the aromatic rings, thus modifying the electron density and affecting the molecular absorbance and fluorescence properties [27]. Together, these interactions not only fix the dyes in certain positions relative to the clay surface but also modify their electronic properties, impacting their optical behaviors in significant ways.

3.1 Characterization of MM-MDH nanoclay

The SEM images in Figure 2 display montmorillonite nanotubes, providing a clear visualization of their tubular structure and surface morphology. SEM allows for the examination of the surface details and the porosity of the nanotubes, which are critical characteristics that influence their chemical reactivity and physical properties. The images likely depict a uniform and consistent tube-like structure, indicating a high degree of purity and structural integrity [28]. This morphology is significant because the surface area and pore structure of montmorillonite nanotubes are key factors that determine their effectiveness. The TEM images of montmorillonite (Figure 3), displayed at different magnifications, provide insight into the internal structure and wall thickness of the nanotubes. TEM is employed to gain a deeper understanding of the ultrastructural features of these nanomaterials. The varying magnifications help highlight the layered silicate structures typical of montmorillonite and halloysite, which are not as easily discernible in SEM images [29]. These images are crucial for assessing the nanotubes' dimensional properties, including inner and outer diameter and wall thickness, which can significantly influence their loading capacity and release characteristics in drug delivery applications. The detailed visualization provided by SEM and TEM plays a pivotal role in the ongoing development and utilization of these nanomaterials in various scientific and industrial fields [30].

Figure 4 presents the FT-IR spectroscopy results for montmorillonite nanotubes. Broad peaks at 3,400 cm^{-1} typically indicate the O–H stretching vibrations, suggesting the presence of hydroxyl groups or water molecules within the nanotube structure. This is common in clays due to their hydrophilic nature and the ability to intercalate water molecules between the layers. The sharp peaks around 1,630 cm^{-1} are characteristic of O–H bending vibrations, often associated with water absorbed in the material. The peaks at 1,000–1,100 cm^{-1} are indicative of Si–O stretching vibrations in the silicate layers, fundamental to the structure of montmorillonite [31]. The sharpness and position of these peaks can give insight into the degree of order in the silicate framework and any substitutions within the lattice. The lower frequency peaks (below 600 cm^{-1}) can be attributed to metal–oxygen bonds, such as Al–O and Mg–O [32], which are integral to the octahedral and tetrahedral sheets of the montmorillonite structure. The FT-IR spectrum of montmorillonite nanotubes confirms the complex structure of these materials, highlighting their potential for

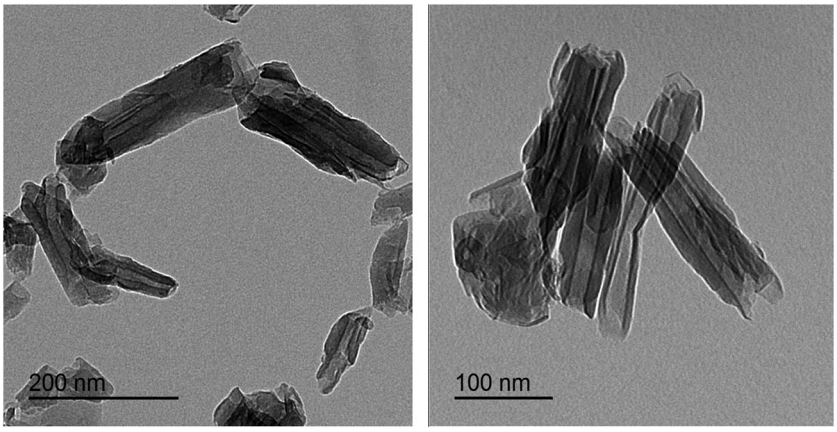

Figure 3: TEM analysis of MM-MDH nanoclay across multiple magnifications.

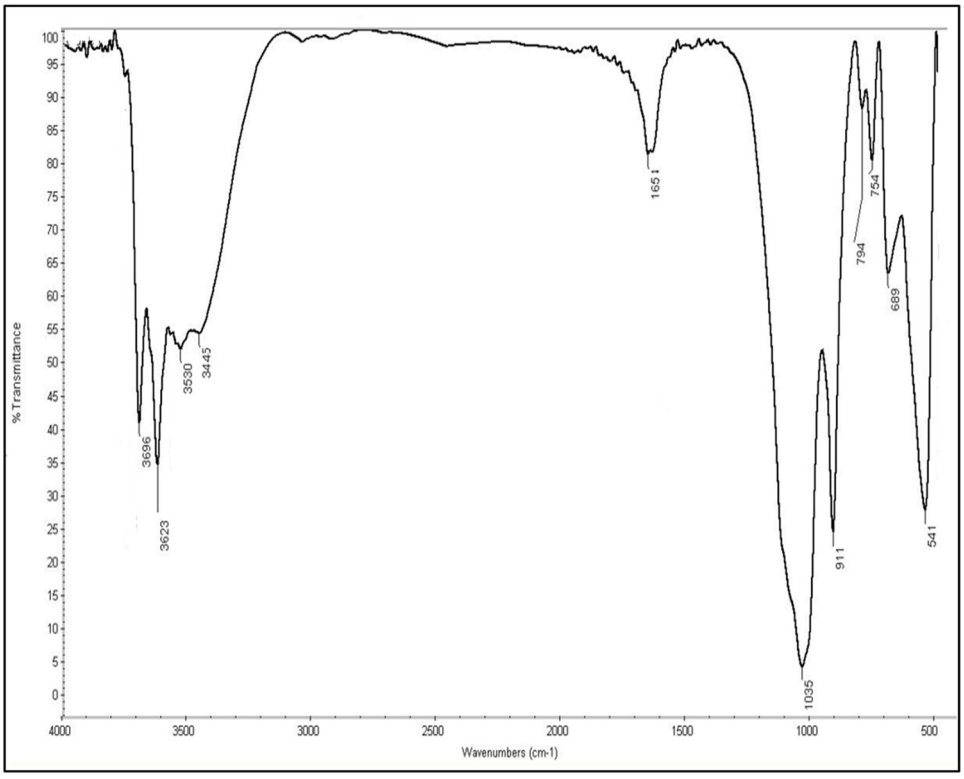

Figure 4: FT-IR of MM-MDH nanoclay.

various applications. The presence of functional groups like hydroxyls suggests their capability for further chemical modifications or functionalization, which could be beneficial in applications ranging from catalysis to drug delivery systems. Additionally, the spectral features indicating water content are crucial for applications in the removal of toxic dyes.

Figure 5 displays the XRD pattern of montmorillonite nanoclay. The peak around 7° (2θ) corresponds to the (001) basal reflection of montmorillonite, indicating the interlayer spacing of the clay [33]. The position and intensity of this peak are important for understanding the layer structure and the degree of swelling or intercalation within the clay layers. The peaks between 19° and 25° (2θ) are generally associated with the quartz impurities in the clay and the crystalline silica components [34]. The presence of these peaks indicates that the nanoclay contains quartz as a minor phase, which is common in natural clays. The sharp peak at 35° (2θ) typically corresponds to the (004) plane of the crystalline silica within montmorillonite, providing further evidence of the crystalline nature of the silica impurities [35]. The broad peak around 62° (2θ) can be attributed to the overlapping of several minor crystalline phases, possibly including various metal oxides that are often present as trace components in montmorillonite [36]. The XRD pattern of montmorillonite nanoclay reveals its semi-crystalline nature and provides insights into its structural components. The prominent basal spacing peak at a low angle suggests a well-defined layer structure, which is characteristic of smectite clays like montmorillonite [37]. This feature is particularly significant because it affects the clay's ability to absorb and intercalate various ions and molecules, which is essential for applications in catalysis, drug delivery, and environmental remediation. The presence of quartz and other crystalline phases indicates the natural origin of the

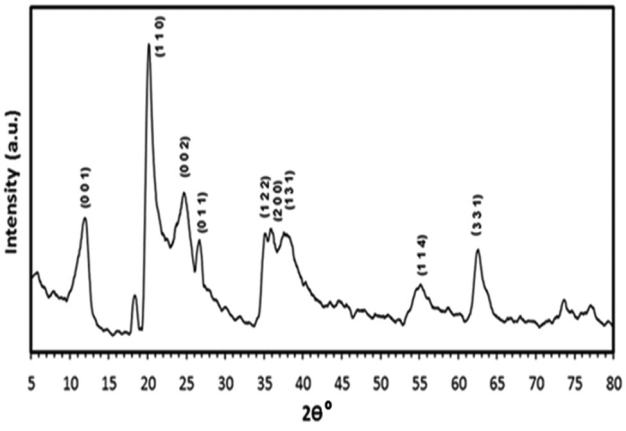

Figure 5: XRD spectra of MM-MDH nanoclay.

clay and suggests that it may have properties influenced by these minor components, such as mechanical strength and thermal stability [38]. Understanding these impurities is crucial for applications where purity and phase composition affect the material's performance.

Figure 6 illustrates the BET surface area analysis of montmorillonite nanoclay, conducted at a temperature of 77 K. The curve starts with a steep rise at lower relative pressures, indicating monolayer adsorption of nitrogen gas. This initial portion is crucial as it reflects the accessible surface area of the montmorillonite nanoclay. As the relative pressure increases, the slope of the curve becomes moderate, suggesting the beginning of multilayer adsorption up to the point where the curve starts to plateau [39]. Towards higher pressures, the isotherm plateaus, indicating that the maximum adsorption capacity has been reached, and the pores are filled with nitrogen gas. The specific surface (BET) was calculated to be 76.4 $m^2 g^{-1}$. The significant rise at low pressures suggests a high surface area, which is characteristic of clays with fine particle sizes and open structures [40]. High surface areas are beneficial for applications requiring efficient interaction with other substances, such as in catalysis or adsorption processes. The shape of the isotherm can give indications about the pore size distribution. The montmorillonite nanoclay likely possesses a range of pore sizes, as inferred from the continuous adsorption beyond the monolayer formation, suggesting the presence of mesopores [41]. The high surface area and porosity make montmorillonite nanoclay an excellent candidate for dye removal.

3.2 The effect of pH on the removal of AR and MB dyes

Figure 7 illustrates the effect of pH on the adsorption of AR and MB dyes using MM-MDH nanoclay, detailing the percentage adsorption across a pH range from 2 to 10. The graph shows a high adsorption percentage for AR dye at acidic conditions, particularly at a pH of 2, where adsorption peaks. The adsorption sharply declines as the pH increases, with a significant drop noted between pH 3 and 6 and continuing to decrease up to pH 10. This trend suggests that the acidic environment enhances the electrostatic attraction between the negatively charged dye molecules and the positively charged sites on MM-MDH nanoclay [42]. At higher pH levels, the surface charge of the nanoclay may become more negative, reducing the electrostatic attraction to the anionic dye molecules, thereby decreasing adsorption efficiency [23]. In contrast, the adsorption of MB dye increases with rising pH, reaching its maximum around pH 8 and stabilizing thereafter. This indicates that the basic conditions favor the adsorption of this cationic dye. The increase in adsorption with pH could be attributed to the increased negative charge on the nanoclay's surface under alkaline conditions [43], which enhances the attraction to the positively charged MB dye molecules. The results indicate that adjusting the pH can significantly affect the adsorption capacity and efficiency, suggesting a need for precise pH control in treatment facilities to maximize dye removal and enhance the sustainability of the process.

3.3 Influence of MM-MDH nanoclay mass on adsorption of dyes

Figure 8 depicts the influence of MM-MDH nanoclay mass on the adsorption efficiency for AR and MB dyes, conducted using a constant dye concentration (20 mg/L for AR and 8 mg/L for MB). The graph shows the adsorption

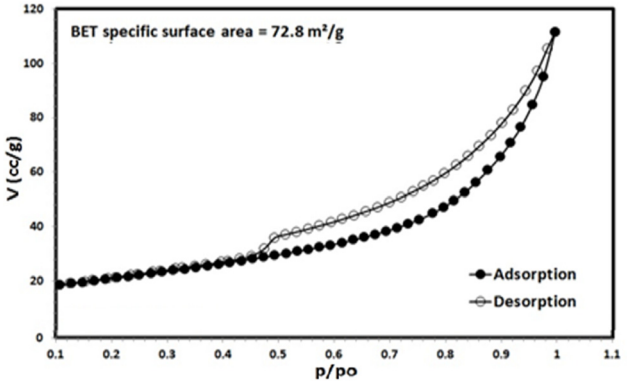

Figure 6: BET surface area of MM-MDH nanoclay at 77 K.

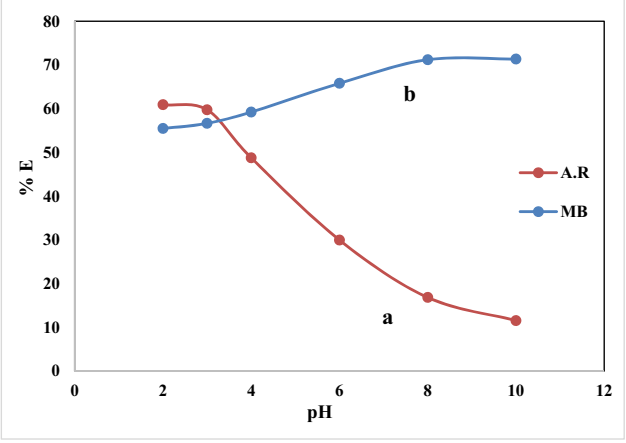

Figure 7: Impact of pH on dye adsorption percentages for AR (a) and MB (b) using MM-MDH nanoclay; 0.01 ± 0.002 g for AR and 0.0075 ± 0.002 g for MB.

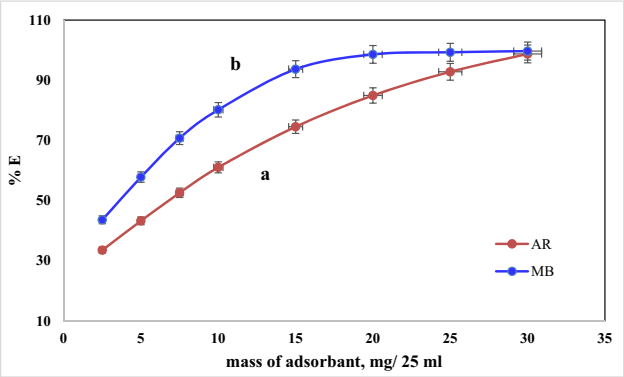

Figure 8: Effect of MM-MDH nanoclay quantity on the adsorption rates of dyes AR (a) and MB (b) over a 120-min duration at 22°C.

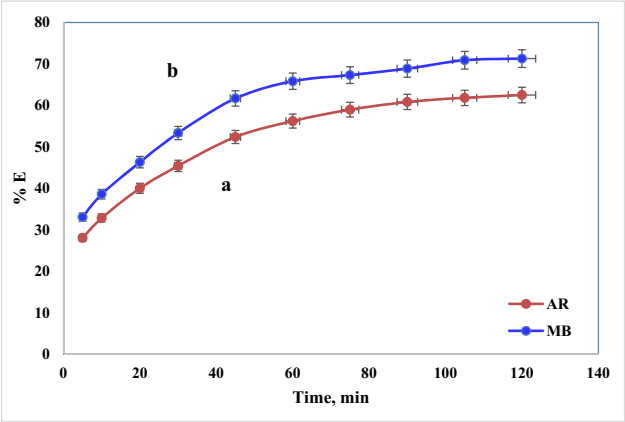

Figure 9: Effect of varying shaking durations on dye removal efficiency for AR (a) and MB (b) using MM-MDH nanoclay at 22°C.

percentage increasing as the dose of MM-MDH nanoclay is increased from 2.5 to 30 mg for both dyes. The adsorption percentage of AR dye increases dramatically from 33.5% at a 2.5 mg dose of nanoclay to 98.7% at a 30 mg dose. This steep increase suggests a significant enhancement in adsorption capacity with the increase in nanoclay amount. Similarly, MB dye shows an increase in adsorption from 43.6% at the lowest nanoclay dose to 99.6% at the highest dose. The adsorption efficiency improves consistently as the dose increases. As the amount of MM-MDH nanoclay increases, so does the total available surface area. More surface area provides more active sites for dye molecules to adhere to, which enhances the adsorption capacity [44]. Higher doses of nanoclay improve the likelihood that dye molecules encounter an available adsorption site, thus reducing the probability of dye molecules remaining in the solution. The primary mechanism here appears to be physical adsorption, where dye molecules are trapped on the surface of nanoclay particles. The findings underscore the importance of optimizing nanoclay dosing in treatment processes to maximize dye removal while considering economic factors. These results could guide the development of scaled-up water treatment protocols that use MM-MDH nanoclay as an adsorbent for removing dye pollutants from industrial effluents.

3.4 Influence of shaking time on adsorption of dyes

Figure 9 demonstrates the effect of shaking time on the adsorption percentages of AR dye and MB dye by MM-MDH nanoclay at a temperature of 22°C. The graph presents time intervals ranging from 5 to 120 min and showcases how the adsorption efficiency changes over these intervals for both dyes. The adsorption of AR dye starts at a moderate level and significantly increases with time, peaking at 120 min. This increase is gradual, indicating that the interaction between the dye and the nanoclay surfaces strengthens over time [45]. Similarly, MB dye shows an increase in adsorption efficiency as time progresses, with the highest adsorption also occurring at the end of the 120-min interval. The pattern of increase is steady, suggesting a continuous accumulation of dye on the nanoclay. The increase in dye removal over time can be attributed to the kinetics of the adsorption process, where initially, a large number of active sites are available, and over time, these sites gradually become occupied [21]. The continuous increase up to 120 min suggests that the saturation point of the nanoclay is not reached within this duration for both dyes. This implies that longer contact times could potentially lead to even higher adsorption efficiencies until all active sites are filled.

3.5 Influence of temperature on adsorption of dyes

Figure 10 illustrates the effect of temperature on the adsorption efficiency of AR dye and MB dye using MM-MDH nanoclay. This graph presents the adsorption percentages at various temperatures, ranging from 10 to 50°C. The adsorption efficiency of AR dye increases as the temperature rises from 10 to 50°C. Starting at a relatively low percentage of 10°C, there is a significant improvement in adsorption as the temperature increases, demonstrating higher efficiency at elevated temperatures. Similarly, MB dye shows an increase in adsorption percentage with temperature. The adsorption starts at a moderate level of 10°C

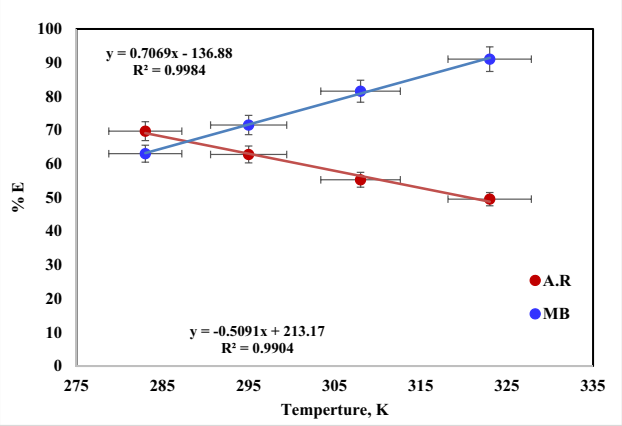

Figure 10: Temperature influence on the removal efficiency of dyes AR and MB using MM-MDH nanoclay over 120 min.

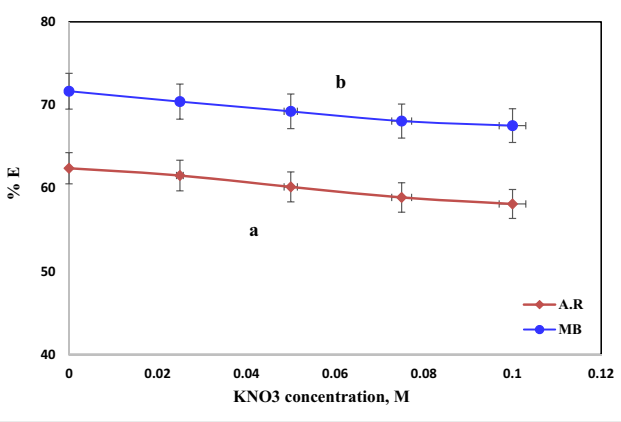

Figure 11: Impact of KNO_3 concentration on dye removal efficiency of AR (a) and MB (b) using MM-MDH nanoclay at 22°C.

and progressively increases, reaching its peak at 50°C. Higher temperatures provide more kinetic energy to the dye molecules, increasing their movement and the probability of contacting the adsorbent sites on MM-MDH nanoclay [41]. This enhanced movement helps overcome any resistance to mass transfer between the aqueous phase and the adsorbent surface. Temperature influences both the adsorption capacity and the rate of adsorption. For physisorption, increased temperature typically enhances the rate of adsorption until a certain point, after which the adsorptive forces may weaken [46]. However, for chemisorption, which may also play a role here, higher temperatures could promote stronger and more stable chemical interactions between the dye molecules and the nanoclay [47]. While higher temperatures can increase adsorption rates, they can also cause increased desorption [48]. In this case, the increasing trend suggests that the adsorption effects are dominant over desorption up to 50°C for both dyes. The findings indicated that increasing the temperature of the solution significantly enhanced the removal efficiency of MB dye by MM-MDH nanoclay, as illustrated in Figure 10. This trend supports the conclusion that the adsorption process is endothermic [45]. Raising the temperature of the solution resulted in reduced efficacy of AR dye removal by MM-MDH nanoclay, as illustrated in Figure 10. This trend indicates that the adsorption process is exothermic [45].

3.6 Influence of KNO_3 on the removal of dyes

Figure 11 demonstrates the impact of KNO_3 concentration on the adsorption efficiency of AR and MB dyes using MM-MDH nanoclay at a constant temperature of 22°C. The figure tracks the change in dye removal percentage as the concentration of KNO_3 varies. The removal efficiency of AR dye is adversely affected by increasing concentrations of KNO_3. The graph shows a noticeable decline in adsorption percentage as the KNO_3 concentration increases. In contrast, the removal efficiency of MB dye appears less affected by changes in KNO_3 concentration, displaying relatively stable adsorption percentages across the different concentrations of KNO_3. The KNO_3 alters the ionic strength of the solution, which can affect the electrostatic interactions between the dye molecules and the nanoclay [49]. For AR dye, the increase in ionic strength likely enhances the competition between the potassium (K^+) and nitrate (NO_3^-) ions and the dye molecules for adsorption sites on the nanoclay, resulting in decreased dye removal efficiency [50]. The presence of KNO_3 may also screen the charges on the nanoclay surface, reducing its ability to attract and bind dye molecules through electrostatic forces [51]. This effect is more pronounced with AR dye due to its specific chemical interactions with the clay. Adding KNO_3 can cause slight changes in the pH and solubility of the dye in water, potentially influencing the dye's state and its interaction with the adsorbent.

The removal mechanism of MB and AR dyes using MM-MDH nanoclay primarily relies on adsorption facilitated by the clay's modified surface. MM-MDH nanoclay, enriched with methyl dihydroxyethyl hydrogenated tallow ammonium, exhibits enhanced adsorption capabilities due to its increased surface area and modified charge properties [52]. For MB, a cationic dye, the adsorption is enhanced under basic conditions (pH 8) due to increased electrostatic attraction between the negatively charged surface of MM-MDH nanoclay and the positively charged dye molecules. Conversely, the removal of AR, an anionic dye, is more efficient in acidic conditions (pH 2) where the clay's surface exhibits a positive charge, facilitating attraction to the negatively charged dye molecules.

3.7 Kinetic study

The study of the kinetic behavior of pollutants like dye species in aqueous solutions using a solid-phase sorbent is critically important as it offers deep insights into chemical reactions and the mechanisms of adsorption steps. The overall rate of transport, including intraparticle diffusion and film diffusion, significantly affects the quantity of dyes adsorbed onto the surface of MM-MDH nanoclay, with the quickest process determining the overall transport rate and thus influencing the amount of dye retained. The experimental results regarding the impact of shaking time allowed for the analysis of the kinetic model for the removal of AR1 and MB dyes using a solid-phase method.

The fractional power function kinetic model is described by the equation below [53]:

$$\ln\ q_t\ =\ \ln\ a\ +b\ \ln\ t. \tag{3}$$

In the experimental setup, q_t represents the amount of dye adsorbed at any given time t, normalized by the mass of MM-MDH nanoclay. Constants a and b, where b is less than 1, are mathematical coefficients integral to the fractional power function equation. When this equation is employed to analyze the adsorption data (refer to Figure 12), it shows compatibility, as evidenced by the R^2 values for AR and MB dyes. The specific values for a and b are listed in Table 1. These results affirm the applicability of the fractional power function kinetic model in describing the adsorption behaviors of AR and MB dyes on the surface of MM-MDH nanoclay.

A crucial formula utilized to analyze the adsorption rate is known as the Lagergren equation. The most popular formulas for describing adsorption rates in liquid-phase methods is the Lagergren equation or pseudo-first order, and the next equation was employed [54,55]:

Table 1: The parameters for various kinetic models for removal of AR and MB dye onto MM-MDH nanoclay at 22°C

Fractional power function kinetic model				
	a	***b***	***ab***	R^2
AR	9.116	0.267	2.433	0.991
MB	5.847	0.257	1.501	0.985
The pseudo-first-order kinetic (Lagergren) model				
	$q_{e,\ exp}$ (mg/g)	$q_{e,\ calc}$ (mg/g)	k_1	R^2
AR	31.26	26.79	0.04	0.978
MB	19.01	16.21	0.043	0.967
The pseudo-second-order kinetic model				
	$q_{e,\ exp}$ (mg/g)	$q_{e,\ calc}$ (mg/g)	k_2	R^2
AR	31.26	34.25	2.4×10^{-3}	0.997
MB	19.01	20.83	4.4×10^{-4}	0.998
Elovich kinetic model				
	α (g/mg min)	***β*** (mg/g min)		R^2
AR	0.251	6.103		0.993
MB	0.514	3.601		0.989

$$\log(q_e - q_t) = \log q_e - \frac{K_{lag}}{2.303}t. \tag{4}$$

The amount of dyes adsorbed per unit weight of MM-MDH nanoclay at equilibrium is denoted by q_e, while q_t represents the amount of dyes adsorbed per unit weight of the nanoclay at any given time t. The constant K_{Lag} indicates the rate of the first-order reaction. A plot of log ($q_e - q_t$) versus time (shown in Figure 13) reveals a linear trend. The values for K_{Lag}, q_e, and the coefficient of determination R^2 concerning the adsorption of AR and MB dyes

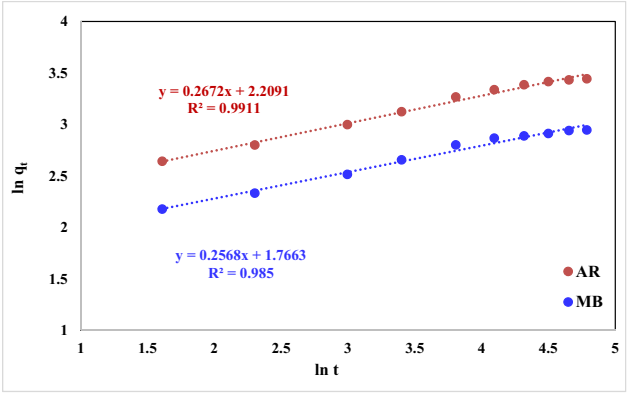

Figure 12: Fractional power model curves for dye species using MM-MDH nanoclay under conditions specified in batch extraction.

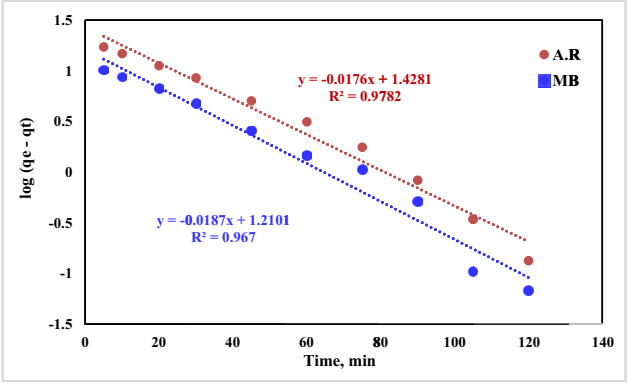

Figure 13: Lagergren kinetics curve for AR and MB dye absorption by MM-MDH nanoclay over time, with experimental conditions detailed in the batch extraction phase.

using MM-MDH nanoclay are detailed in Table 1. The observed data suggest that the first-order kinetics model does not adequately describe the adsorption behavior of AR and MB dye species on MM-MDH nanoclay [56].

The pseudo-second-order kinetic model can be represented through the equation provided below. This model operates under two key assumptions: first, the total number of available binding sites is defined by the equilibrium concentration of the adsorbate, and second, the concentration of the adsorbate does not change during the process. The following equation illustrates this model [57]:

$$\frac{t}{q_t} = \frac{1}{k_2 q_e^2} + \left(\frac{1}{q_e}\right)t. \tag{5}$$

In the formula, q_e represents the equilibrium concentration of dyes absorbed per unit weight of MM-MDH nanoclay, while q_t denotes the concentration at any given time t. The variable k_2 stands for the pseudo-second-order rate constant. Plots of t/q_t versus t displayed linearity under these conditions, as shown in Figure 14. By analyzing the intercept and slope of these plots for AR and MB dyes, values for the second-order rate constant (k_2) and the equilibrium capacity (q_e) were calculated and are documented in Table 1. The results confirm that the pseudo-second-order kinetic model effectively describes the adsorption dynamics of AR and MB dyes on MM-MDH nanoclay. This model's applicability is influenced by several experimental parameters including contact time, pH levels, dye concentration, and ambient temperature [58].

The kinetic model described is derived from the Elovich equation [42], commonly employed to quantify adsorption capacities. This model is particularly applicable to chemisorption processes and proves effective in scenarios featuring heterogeneously adsorbing surfaces. The model is mathematically represented by the following equation:

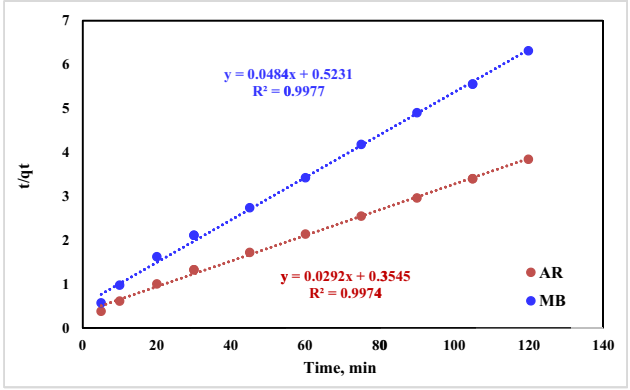

Figure 14: Kinetic adsorption curves for AR and MB dyes on MM-MDH nanoclay over time with previously described batch conditions.

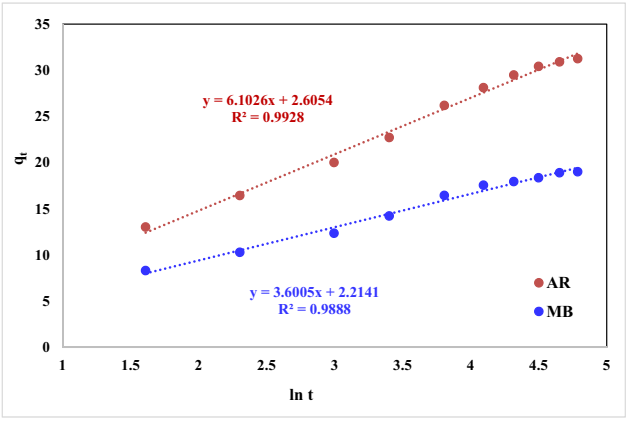

Figure 15: Elovich model dynamics for AR and MB dye adsorption on MM-MDH nanoclay over time, with experimental conditions specified in previous batch adsorption descriptions.

$$q_t = \beta \ln(\alpha\beta) + \beta \ln t. \tag{6}$$

The parameters α and β, representing the initial adsorption rate and the desorption coefficient, respectively, were quantified using the Elovich model. Linear relationships between q_t and ln(t) are depicted in Figure 15. From these plots, the values of the α and β coefficients were calculated using the slopes and intercepts. The derived data are detailed in Table 1.

The Weber and Morris model of intraparticle diffusion for AR and MB dyes removal by MM-MDH nanoclay is derived as follows:

$$q_t = K_{id}(t)^{1/2} + C, \tag{7}$$

where k_{id} is the intra-particle diffusion rate constant (mg/g $min^{1/2}$) and C (mg/g) is a constant proportional to the thickness of the boundary layer. Applying the intra-particle diffusion model to all the adsorption experimental data in Figure 16 with zero intercept converged well and had

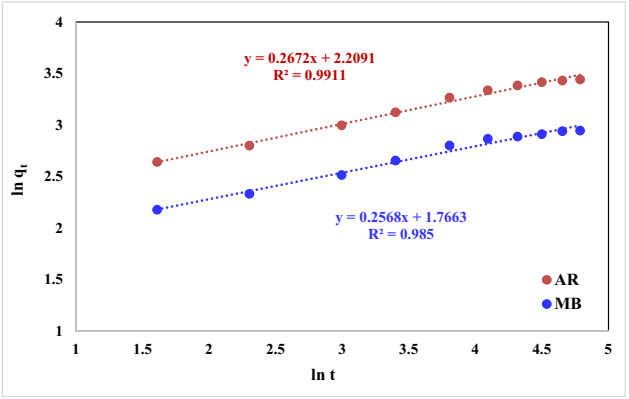

Figure 16: Graphical representation of intra-particle diffusion for AR and MB dye removal via solid-phase extraction.

straight lines pass through the origin as well as presented in the figure, which indicate the not suitability of the intra-particle diffusion model for all the experimental data and the value of K_{id} was equal 2.593 for AR and equal 1.562 for MB with correlation coefficient (R^2) 0.911 for AR1 and 0.895 for MB, respectively, as is illustrated in Figure 16.

The kinetic analysis, drawing from correlation coefficients displayed in Table 1 and data derived from various models, including fractional power function, Lagergren pseudo-first-order, pseudo-second-order, and Elovich, indicates that the pseudo-second-order model is most suitable for characterizing the adsorption kinetics of dye species AR and MB on MM-MDH nanoclay.

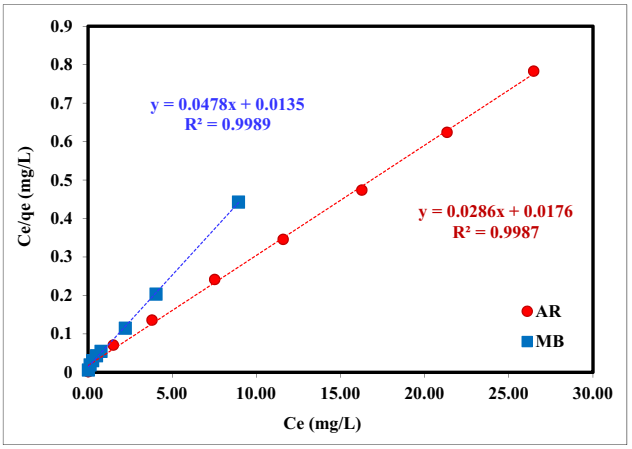

Figure 18: Langmuir adsorption isotherms for AR and MB dyes on MM-MDH nanoclay at 22°C.

3.8 Adsorption isotherms for AR1 and CV dyes uptake by MM-MDH nanoclay

Figure 17 illustrates the adsorption capacity (q_e) of AR and MB dyes onto MM-MDH nanoclay against their equilibrium concentrations (C_e) at a constant temperature of 22°C. This plot is critical for understanding the adsorption isotherms, which describe how dyes interact with the adsorbent at a constant temperature. For AR, the adsorption capacity (q_e) increases with increasing equilibrium concentration (C_e) up to a certain point, after which it may plateau. This suggests that more sites on the nanoclay become occupied until saturation is reached. Similarly, MB shows an increase in q_e with C_e. The plot would typically show how efficiently MM-MDH nanoclay adsorbs MB dye from the solution, potentially reaching a plateau as the available adsorption sites become fully occupied. Critical analysis was done on the retention patterns throughout a range of equilibrium values (5–40 mg/L) for AR and range values of (1–15 mg/L) for MB dyes via the aquatic solutions on

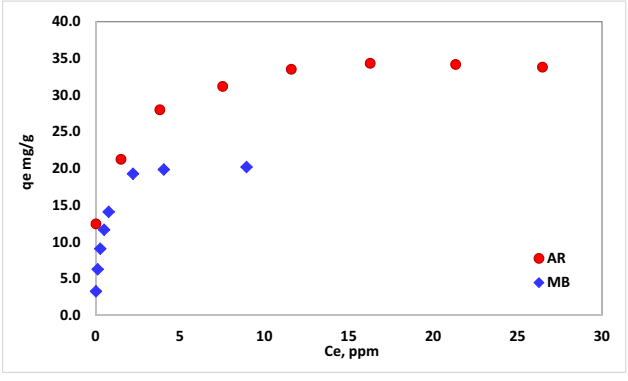

Figure 17: Graphical representation of AR and MB dye adsorption on MM-MDH nanoclay (mg/g) versus equilibrium concentration (C_e) at 22°C.

the utilized sorbent under ideal conditions. The amount of dyes retained in the solution showed a linear correlation with the quantity of dyes adsorbed by the MM-MDH nanoclay at moderate sample concentrations. The adsorption capacity for AR was determined to be 34.33 ± 0.12 mg/g, and for MB, it was 20.19 ± 0.09 mg/g onto MM-MDH nanoclay. The behavior of both dyes can be analyzed using adsorption isotherm models like Langmuir and Freundlich, which describe how contaminants interact with adsorbent surfaces. The initial steep portion of the curve typically indicates that a large number of available sites are being quickly occupied [59]. As the curve flattens, it indicates that fewer sites are available, and the adsorption process becomes limited by the availability of sites rather than the concentration of the dye [60]. The molecular structure and chemical properties of AR and MB dyes influence their interaction with MM-MDH nanoclay. AR, being an anionic dye, and MB, a cationic dye, may interact differently with the charged sites on the nanoclay, affecting the adsorption capacity and efficiency.

The next form of linearity represents the Langmuir isotherm equation applied to the retention of AR and MB dyes on SP sorbent [61]:

$$\frac{C_e}{q_e} = \frac{1}{q_m k_L} + \frac{C_e}{q_m}. \quad (8)$$

The term C_e denotes the equilibrium concentration (mg/L) of dyes (AR and MB) within the solution being tested, while q_e refers to the amount of the dye adsorbed per unit mass of the adsorbent at equilibrium (mg/g). The parameters q_m and k_L are known as Langmuir constants. q_m correlates to the maximum adsorption capacity of the adsorbent for forming a monolayer, whereas K_L is the equilibrium constant reflecting the energy of adsorption independent of temperature. The plot of C_e/q_e against C_e

for various concentrations of AR and MB dyes on MM-MDH nanoclay was found to be linear, as shown in Figure 18, with correlation coefficients (R^2) of 0.9987 for AR dye and 0.9989 for MB dye. This suggests that the adsorption of these dyes on the surface of MM-MDH nanoclay is uniform and conforms well to the Langmuir adsorption model. The values for q_m and K_L were calculated from the slope and intercept of this linear plot and are presented in Table 2. Additionally, the dimensionless separation factor R_L is a key feature of this model and is defined as follows:

$$R_L = \frac{1}{1 + K_L C_o}. \tag{9}$$

R_L values for the adsorbent equal 0. 0.075 for AR and equal 0.307 for MB dyes ($0 < R_L < 1$), which indicates favorable monolayer adsorption [62].

The retention behavior of AR and MB dyes from aqueous solution onto the used sorbents was subjected to the Freundlich system represented in the next form of linearity [63]:

$$\log q_e = \log K_F + (1/n) \log C_e. \tag{10}$$

The Freundlich constants, K_F and $1/n$, relate to the maximum capacity of solute sorption (mg/g). These parameters are defined where q_e represents the equilibrium concentration of AR and MB dyes adsorbed on the MM-MDH nanoclay per unit mass (mg/g), and C_e indicates the concentration of dyes remaining in the aqueous solution (mg/L). The estimated values for K_F and $1/n$ are presented in Table 2, derived from the intercept and slope observed in Figure 19. The $1/n$ value was found to be equal to 0.151 for AR and equal to 0.329 for MB dyes, which are a lesser amount than unity ($1/n < 1$); thus, sorbents' surfaces were favorable sorption of AR and MB dyes by the MM-MDH nanoclay. The correlation coefficients (R^2) of the Freundlich model for AR and MB dyes do not have good values, which recommends that the adsorption model was better explained by the Langmuir model.

Table 2: The parameter of Langmuir and Freundlich isotherm models for the retention of AR and MB dyes on MM-MDH nanoclay at 22°C

Models of sorption isotherms		AR dye	MB dye
Langmuir	q_m (mg/g)	34.96	20.92
	K_L (L/g)	0.615	0.282
	R_L	0.075	0.307
	R^2	0.9987	0.9989
Freundlich	K_F (mg/g)	21.97	13.18
	$1/n$	0.151	0.329
	R^2	0.9765	0.9626

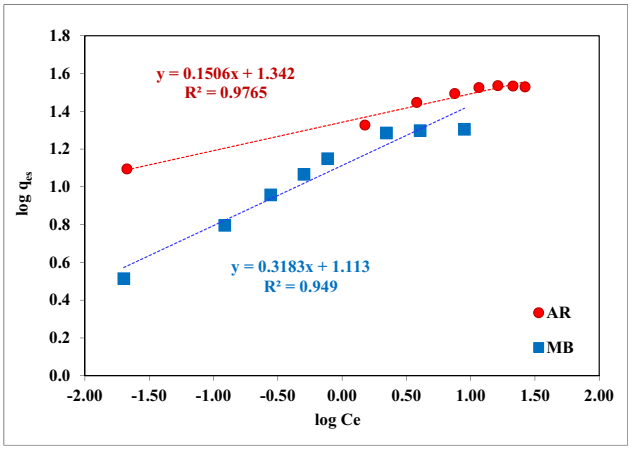

Figure 19: Graph of logarithmic adsorption capacity versus equilibrium concentration for AR and MB dyes on MM-MDH nanoclay at 22°C (Freundlich isotherms).

3.9 Thermodynamic properties of BG and AR dyes adsorption using MM-MDH nanoclay

The absorption of AR and MB dyes using MM-MDH nanoclay was extensively investigated across a temperature spectrum from 283 to 323 K to assess dye retention by MM-MDH nanoclay. Thermodynamic parameters such as enthalpy (ΔH), entropy (ΔS), and Gibbs free energy (ΔG) were calculated using specific equations [64]:

$$\ln K_c = \frac{\Delta H}{RT} + \frac{\Delta S}{R}, \tag{11}$$

$$\Delta G = \Delta H - T\Delta S, \tag{12}$$

$$\Delta G = RT \ln K_c, \tag{13}$$

where the temperature is T (Kelvin), the gas constant is R, and the equilibrium constant is K_c. The following equation was used to compute the values of constant K_c for the adsorption of AR and MB dyes:

$$k_c = \frac{C_a}{C_e}, \tag{14}$$

The term C_e refers to the equilibrium concentration of AR and MB dyes in an aqueous solution, expressed in milligrams per liter (mg/L), whereas C_a denotes the amount of AR and MB dyes adsorbed on the solid surface at equilibrium, also measured in milligrams per liter (mg/L).

Figure 20 presents two curves showing the natural logarithm of the distribution coefficient ($\ln K_c$) against the inverse of temperature (multiplied by 1,000, i.e., 1,000/T) for the uptake of two dyes, AR and MB, from an aquatic solution using MM-MDH nanoclay. The graph displays two contrasting trends: the uptake of AR dye decreases exponentially with

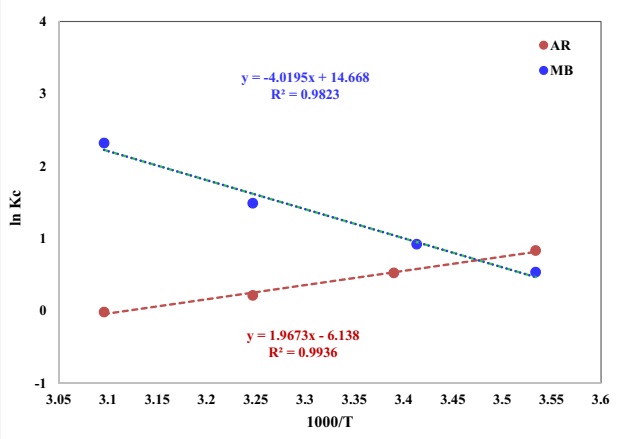

Figure 20: Logarithmic plots of equilibrium constants (ln K_c) versus inverse temperature (1,000/T) for AR and MB dye adsorption from aqueous solutions by MM-MDH nanoclay.

increasing temperature, while the uptake of MB dye increases exponentially as temperature rises. For AR, the negative slope indicates that the adsorption is exothermic; higher temperatures reduce the adsorption efficiency [65]. This could be due to the weakening of interactions between the dye and the adsorbent at higher temperatures. For MB, the positive slope suggests endothermic adsorption; higher temperatures enhance the adsorption efficiency. This could be due to increased molecular motion, improving interactions between the dye and adsorbent sites [66]. The decrease in ln K_c with increasing temperature could be attributed to the desorption of AR from the nanoclay, possibly due to the breakdown of weaker physical bonds like hydrogen bonds or van der Waals forces at higher temperatures. The increase in ln K_c with temperature (MB dye) suggests that stronger or additional chemical bonds (e.g., covalent or ionic) might be forming at higher temperatures, enhancing adsorption. The differing trends for AR and MB with temperature change are rooted in the thermodynamic properties of the adsorption process. These include changes in enthalpy (ΔH) and entropy (ΔS), which dictate whether adsorption becomes more or less favorable with temperature. The specific characteristics of MM-MDH nanoclay, such as surface area, pore size, and functional groups, also play significant roles in how it interacts differently with AR and MB dyes under varying thermal conditions.

3.10 Practical investigation

To assess the efficacy of MM-MDH nanoclay solid phase in adsorbing and removing dye contaminants from water, it is essential to test its application in real water scenarios. Investigations were carried out on three different water types: seawater, wastewater, and tap water. These samples were initially analyzed for the presence of AR and MB dyes, which were not detectable by UV–Vis spectroscopy. Subsequently, each sample was enhanced with 20 mg/L of AR dye and treated with 30 mg of MM-MDH nanoclay at a pH of 2. The mixtures were agitated for 120 min at a temperature of 295 K. In a similar experimental setup, but with a pH adjusted to 8, the samples were spiked with 8 mg/L of MB dye and treated with the same amount of nanoclay under identical conditions. Figure 21 shows the efficiency of AR and MB dye removal by MM-MDH nanoclay from three different water types: tap water, wastewater, and seawater. The experiment was conducted under controlled conditions with a fixed volume, contact time, pH, temperature, amount of nanoclay, and initial dye concentrations. The data show that AR dye removal efficiency in tap water, wastewater, and seawater is 96.68, 94.05, and 92.30%, respectively, while MB dye removal efficiency is slightly higher at 97.10, 94.76, and 93.04% for the same water types. Both AR and MB dyes show the highest removal efficiencies in tap water and the lowest in seawater. This trend suggests that the ionic composition and possibly organic content of seawater interfere more with dye removal compared to the relatively cleaner tap water. The high-efficiency rates across all water types highlight the effectiveness of MM-MDH nanoclay as an adsorbent for both dyes under varying water qualities. The differing pH conditions for AR (pH 2) and MB (pH 8) during testing likely affect the charge interactions between the dyes and the nanoclay, influencing the removal efficiency.

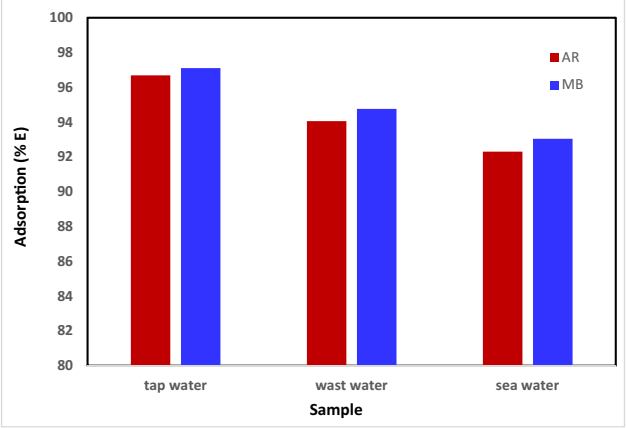

Figure 21: Removal efficiency of AR and MB dyes using MM-MDH nanoclay across three real-world samples (experimental conditions: 25 mL solution, contact time = 120 min, pH solution = 2, temperature = 295 K, 30 mg of MM-MDH nanoclay and 20 mg L^{-1} concentration for AR dye, and for MB dye 25 mL solution, contact time = 120 min, pH solution = 8, temperature = 295 K, 30 mg of MM-MDH nanoclay, and 8 mg L^{-1} concentration).

Both wastewater and seawater contain more competitive ions and possibly organic matter that can occupy adsorption sites on the nanoclay or interact with the dyes, reducing the efficiency of dye removal compared to tap water [67]. The ionic strength of seawater could lead to a shielding effect, reducing the effective charge interactions necessary for optimal dye adsorption on nanoclay [68]. The chemical nature and the amount of competing substances in wastewater and seawater likely interfere with the adsorption process, making it less efficient than in tap water. The consistency in high removal efficiencies across different waters suggests that MM-MDH nanoclay has a robust adsorption capacity, although slightly reduced in more complex matrices like seawater.

Figure 22 illustrates the reusability of MM-MDH nanoclay in the removal of AR and MB dyes over four cycles. Each cycle involves treating 25 mL of dye solution under controlled experimental conditions, using 30 mg of MM-MDH nanoclay at specified pH and temperature settings for each dye. The data reveal that AR dye removal efficiency using MM-MDH nanoclay decreases over four cycles, starting at 98.43% in the first cycle and reducing to 92.58% by the fourth cycle. Similarly, MB dye removal efficiency starts at 99.14% in the first cycle and diminishes to 93.99% in the fourth cycle, showcasing a gradual decline in the adsorbent's performance with repeated use. The gradual decline in removal efficiency for both dyes over successive cycles suggests a reduction in the adsorptive capacity of MM-MDH nanoclay. This trend is typical for adsorbent materials, where initial cycles utilize more active sites, and subsequent cycles exhibit saturation and reduced efficiency. MB dye consistently shows slightly higher removal efficiencies compared to AR dye across all cycles. This might indicate a stronger affinity of MB dye molecules for the binding sites available on MM-MDH nanoclay, possibly due to differences in molecular structure or interactions under the experimental pH conditions. Incomplete desorption of dyes from the nanoclay between cycles could block sites or alter the surface characteristics, hindering further adsorption efficiency [24]. The stability of the nanoclay under the experimental conditions across multiple cycles could also influence the observed decline in efficiency, where physical or chemical changes to the adsorbent material affect its performance [69]. These findings highlight the potential for using MM-MDH nanoclay as a reusable adsorbent in dye removal applications, although they also indicate the need for regeneration strategies to maintain high efficiency over multiple cycles.

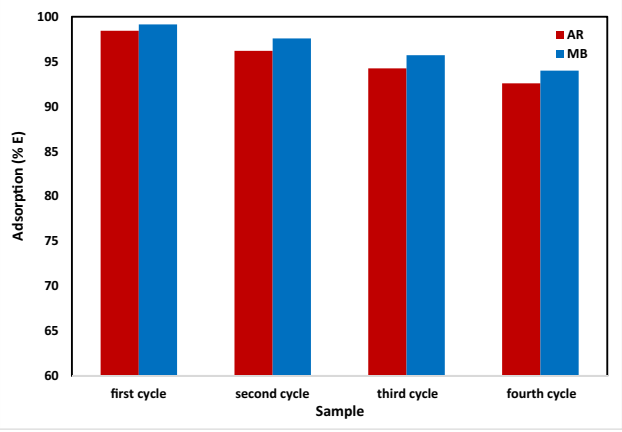

Figure 22: The reusability effect of MM-MDH nanoclay for removal of AR and MB dyes four times, (experimental conditions: 25 mL solution, contact time = 120 min, pH solution = 8, temperature = 295 K, 30 mg of MM-MDH nanoclay and 8 mg L^{-1} concentration for MB dye, and for the AR dye 25 mL solution, contact time = 120 min, pH solution = 2, temperature = 295 K, 30 mg of MM-MDH nanoclay and 20 mg L^{-1} concentration).

Table 3: Comparison between the MM-MDH nanoclay and other reported adsorbents for removal of AR and MB dyes

Dyes	Solid phase	Uptake capacity	Reference
AR	Black tea leaves	30.3	[5]
AR	Carboxylated alginic acid	9.17	[70]
AR	Ferrous sulfate flocs	6.623	[71]
AR	Activated carbon	18.76	[51]
AR	Halloysite nanoclay	13.89	[42]
AR	Zinc ferrite $Mn_{0.8}Zn_{0.2}Fe_2O_4$ magnetic	49.90	[72]
AR	**MM-MDH nanoclay**	**34.33**	**This work**
MB	Green tea dredge	71.4	[73]
MB	Sugarcane bagasse	12.42	[74]
MB	Treated sugarcane bagasse	58.9	[75]
MB	Sodium alginate hydrogel	51.34	[76]
MB	Magnetic chitosan–PEGDE–EDTA composite	5.04	[77]
MB	Activated corn husk waste		[78]
MB	**MM-MDH nanoclay**	**12.5**	**This work**

The performance of MM-MDH nanoclay as a solid adsorbent for extracting AR and MB dyes was assessed against other established adsorbents, focusing on adsorption efficiency and duration. Data presented in Table 3 indicate that MM-MDH nanoclay shows potential as an effective and viable option for the adsorption of AR and MB dyes from solutions.

4 Conclusion

The study successfully demonstrates a simple, eco-friendly method for the removal of toxic dyes, specifically MB and

AR 1, from aqueous solutions using MM-MDH nanoclay. Through systematic investigation, it was found that MM-MDH nanoclay effectively adsorbed these dyes, achieving significant removal within 90 min. The adsorption capacities under optimal conditions were 34.33 mg/g for AR dye and 20.19 mg/g for MB dye. Kinetic studies indicated that the adsorption followed a pseudo-second-order model, while thermodynamic analysis revealed that the process was spontaneous and exothermic for AR dye and spontaneous and endothermic for MB dye. The application of MM-MDH nanoclay in real water samples further validated its high performance in dye removal, maintaining efficiency over multiple cycles. This highlights the potential of MM-MDH nanoclay as a sustainable and effective adsorbent for treating dye-contaminated water, offering a viable solution for industrial wastewater management and environmental protection.

Future research on MM-MDH nanoclay should prioritize evaluating its long-term stability and regeneration capabilities to fully ascertain its practical utility for dye adsorption. Long-term stability studies would involve subjecting the nanoclay to extended periods of use under varying environmental conditions to observe changes in its structural integrity and adsorption capacity. Such studies will provide invaluable data on the material's degradation patterns and lifespan in real-world applications. Furthermore, exploring the regeneration of the nanoclay after dye adsorption is crucial. This would involve developing and optimizing cost-effective and environmentally friendly methods for desorbing adsorbed dyes and rejuvenating the nanoclay's adsorptive properties. Investigating these aspects will enhance our understanding of the nanoclay's reusability and its potential for multiple cycles of use, thereby contributing to sustainability and economic feasibility in industrial applications. This line of inquiry not only extends the practical applications of the nanoclay but also aligns with environmental sustainability goals by reducing waste and the need for continual raw material consumption.

Acknowledgment: The author would like to thank the Deanship of Scientific Research at Shaqra University for supporting this work.

Funding information: Authors state no funding involved.

Author contributions: The current work was designed, drafted, and edited, and the laboratory work was prepared and reviewed by Raja Alruwais.

Conflict of interest: The author declares no conflict of interest.

Ethical approval: The conducted research is not related to either human or animal use.

Data availability statement: The data used to support the findings of this study are available from the corresponding author upon request.

References

[1] Rahmani S, Zeynizadeh B, Karami S. Removal of cationic methylene blue dye using magnetic and anionic-cationic modified montmorillonite: kinetic, isotherm and thermodynamic studies. Appl Clay Sci. 2020;184:105391.

[2] Salih SJ, Kareem ASA, Anwer SS. Adsorption of anionic dyes from textile wastewater utilizing raw corncob. Heliyon. 2022;8(8):e10092.

[3] Alsukaibi AK. Various approaches for the detoxification of toxic dyes in wastewater. Processes. 2022;10(10):1968.

[4] Mansour RAEG, Simeda MG, Zaatout AA. Removal of brilliant green dye from synthetic wastewater under batch mode using chemically activated date pit carbon. RSC Adv. 2021;11(14):7851–61.

[5] Ahmed R, Rafia RR, Hossain MA. Kinetics and thermodynamics of acid red 1 adsorption on used black tea leaves from aqueous solution. Int J Sci. 2021;10(6):7–15.

[6] Ragab A, Ahmed I, Bader D. The removal of brilliant green dye from aqueous solution using nano hydroxyapatite/chitosan composite as a sorbent. Molecules. 2019;24(5):847.

[7] Alqarni SA. The performance of different AgTiO2 loading into poly (3-Nitrothiophene) for efficient adsorption of hazardous brilliant green and crystal violet dyes. Int J Polym Sci. 2022;2022(1):4691347.

[8] Jorfi S, Barkhordari MJ, Ahmadi M, Jaafarzadeh N, Moustofi A, Ramavandi B. Photodegradation of Acid red 18 dye by BiOI/ZnO nanocomposite: A dataset. Data Brief. 2018;16:608–11.

[9] Sonal S, Mishra BK. Role of coagulation/flocculation technology for the treatment of dye wastewater: trend and future aspects. Water Pollution and Management Practices. Singapore: Springer; 2021. p. 303–31.

[10] Rekhate CV, Shrivastava JK. Decolorization of azo dye solution by ozone based advanced oxidation processes: optimization using response surface methodology and neural network. Ozone: Sci Eng. 2020;42(6):492–506.

[11] Ma X, Chen P, Zhou M, Zhong Z, Zhang F, Xing W. Tight ultrafiltration ceramic membrane for separation of dyes and mixed salts (both NaCl/Na2SO4) in textile wastewater treatment. Ind Eng Chem Res. 2017;56(24):7070–9.

[12] Iqbal J, Shah NS, Sayed M, Niazi NK, Imran M, Khan JA, et al. Nanozerovalent manganese/biochar composite for the adsorptive and oxidative removal of Congo-red dye from aqueous solutions. J Hazard Mater. 2021;403:123854.

[13] Osagie C, Othmani A, Ghosh S, Malloum A, Esfahani ZK, Ahmadi S. Dyes adsorption from aqueous media through the nanotechnology: A review. J Mater Res Technol. 2021;14:2195–218.

[14] Anastopoulos I, Pashalidis I, Orfanos AG, Manariotis ID, Tatarchuk T, Sellaoui L, et al. Removal of caffeine, nicotine and amoxicillin from (waste) waters by various adsorbents. A review. J Environ Manag. 2020;261:110236.

[15] Amari A, Mohammed Alzahrani F, Mohammedsaleh Katubi K, Salem Alsaiari N, Tahoon MA, Ben Rebah F. Clay-polymer

nanocomposites: Preparations and utilization for pollutants removal. Materials. 2021;14(6):1365.
[16] Ao C, Zhao J, Li Q, Zhang J, Huang B, Wang Q, et al. Biodegradable all-cellulose composite membranes for simultaneous oil/water separation and dye removal from water. Carbohydr Polym. 2020;250:116872.
[17] Demissie H, An G, Jiao R, Ritigala T, Lu S, Wang D. Modification of high content nanocluster-based coagulation for rapid removal of dye from water and the mechanism. Sep Purif Technol. 2021;259:117845.
[18] Waliullah RM, Rehan AI, Awual ME, Rasee AI, Sheikh MC, Salman MS, et al. Optimization of toxic dye removal from contaminated water using chitosan-grafted novel nanocomposite adsorbent. J Mol Liq. 2023;388:122763.
[19] Marczenko Z. Separation and spectrophotometric determination of elements. 2nd edn. United States: John Wiley and Sons; 1986.
[20] Giovannini G, Rossi RM, Boesel LF. Changes in optical properties upon dye–clay interaction: Experimental evaluation and applications. Nanomaterials. 2021;11(1):197.
[21] Kavil YN, Shaban YA, Alelyani SS, Al-Farawati R, Orif MI, Ghandourah MA, et al. The removal of methylene blue as a remedy of dye-based marine pollution: a photocatalytic perspective. Res Chem Intermed. 2020;46:755–68.
[22] Khan MD, Singh A, Khan MZ, Tabraiz S, Sheikh J. Current perspectives, recent advancements, and efficiencies of various dye-containing wastewater treatment technologies. J Water Process Eng. 2023;53:103579.
[23] Kausar A, Iqbal M, Javed A, Aftab K, Bhatti HN, Nouren S. Dyes adsorption using clay and modified clay: A review. J Mol Liq. 2018;256:395–407.
[24] Al Kausor M, Gupta SS, Bhattacharyya KG, Chakrabortty D. Montmorillonite and modified montmorillonite as adsorbents for removal of water soluble organic dyes: A review on current status of the art. Inorg Chem Commun. 2022;143:109686.
[25] Xiao J, Lv W, Xie Z, Tan Y, Song Y, Zheng Q. Environmentally friendly reduced graphene oxide as a broad-spectrum adsorbent for anionic and cationic dyes via π–π interactions. J Mater Chem A. 2016;4(31):12126–35.
[26] Airinei A, Homocianu MIHAELA, Dorohoi DO. Changes induced by solvent polarity in electronic absorption spectra of some azo disperse dyes. J Mol Liq. 2010;157(1):13–7.
[27] Chen T, Li M, Liu J. π–π stacking interaction: a nondestructive and facile means in material engineering for bioapplications. Cryst Growth Des. 2018;18(5):2765–83.
[28] Largo F, Haounati R, Ighnih H, Malekshah RE, Rhaya M, Ouachtak H, et al. Effective removal of toxic dye from wastewater via advanced modified magnetic sepiolite using combined surfactants SDS/CTAB/Fe3O4@ Sep: Empirical and computational analysis studies. J Mol Liq. 2024;407:125114.
[29] Massaro M, Noto R, Riela S. Past, present and future perspectives on halloysite clay minerals. Molecules. 2020;25(20):4863.
[30] Su D. Advanced electron microscopy characterization of nanomaterials for catalysis. Green Energy Environ. 2017;2(2):70–83.
[31] Madejová J, Balan E, Petit S. Application of vibrational spectroscopy to the characterization of phyllosilicates and other industrial minerals. Advances in the characterization of industrial minerals. 2010.
[32] Jovanovski G, Makreski P. Minerals from Macedonia. XXX. Complementary use of vibrational spectroscopy and X-ray powder diffraction for spectra-structural study of some cyclo-, phyllo-and tectosilicate minerals. A Rev Maced J Chem Chem Eng. 2016;35(2):125–55.
[33] Chen Q, Zhu R, Deng W, Xu Y, Zhu J, Tao Q, et al. From used montmorillonite to carbon monolayer–montmorillonite nanocomposites. Appl Clay Sci. 2014;100:112–7.
[34] Mostafa NY, Mohsen Q, El-Maghraby A. Characterization of low-purity clays for geopolymer binder formulation. Int J Miner Metall Mater. 2014;21:609–19.
[35] Carrado KA, Xu L, Csencsits R, Muntean JV. Use of organo-and alkoxysilanes in the synthesis of grafted and pristine clays. Chem Mater. 2001;13(10):3766–73.
[36] Kinoti IK, Karanja EM, Nthiga EW, M'thiruaine CM, Marangu JM. Review of clay-based nanocomposites as adsorbents for the removal of heavy metals. J Chem. 2022;2022(1):7504626.
[37] Hong H, Churchman GJ, Gu Y, Yin K, Wang C. Kaolinite–smectite mixed-layer clays in the Jiujiang red soils and their climate significance. Geoderma. 2012;173:75–83.
[38] Belghazdis M, Hachem EK. Clay and clay minerals: a detailed review. Int J Recent Technol Appl Sci (IJORTAS). 2022;4(2):54–75.
[39] Yang Q, Xue J, Li W, Hu B, Ma Q, Zhan K, et al. Reconstructions of supercritical CO2 adsorption isotherms and absolute adsorption estimation in nanoporous coals considering volumetric effects and varying adsorbed phase densities. Chem Eng J. 2022;433:133492.
[40] Feng D, Li X, Wang X, Li J, Sun F, Sun Z, et al. Water adsorption and its impact on the pore structure characteristics of shale clay. Appl Clay Sci. 2018;155:126–38.
[41] Zhang T, Wang W, Zhao Y, Bai H, Wen T, Kang S, et al. Removal of heavy metals and dyes by clay-based adsorbents: From natural clays to 1D and 2D nano-composites. Chem Eng J. 2021;420:127574.
[42] Abdel-Fadeel MA, Aljohani NS, Al-Mhyawi SR, Halawani RF, Aljuhani EH, Salam MA. A simple method for removal of toxic dyes such as Brilliant Green and Acid Red from the aquatic environment using Halloysite nanoclay. J Saudi Chem Soc. 2022;26(3):101475.
[43] Geroeeyan A, Niazi A, Konoz E. Removal of Basic Orange 2 dye and Ni2+ from aqueous solutions using alkaline-modified nanoclay. Water Sci Technol. 2021;83(9):2271–86.
[44] Natarajan S, Bajaj HC, Tayade RJ. Recent advances based on the synergetic effect of adsorption for removal of dyes from waste water using photocatalytic process. J Environ Sci. 2018;65:201–22.
[45] Hosseini SA, Daneshvare Asl S, Vossoughi M, Simchi A, Sadrzadeh M. Green electrospun membranes based on chitosan/amino-functionalized nanoclay composite fibers for cationic dye removal: Synthesis and kinetic studies. ACS Omega. 2021;6(16):10816–27.
[46] Younas M, Sohail M, Leong LK, Bashir MJ, Sumathi S. Feasibility of CO2 adsorption by solid adsorbents: a review on low-temperature systems. Int J Environ Sci Technol. 2016;13:1839–60.
[47] Kouda I, Seddik NB, Laaziz A, Hadri M, Draoui K, Elmidaoui A. Efficient removal of cationic dye from wastewater using novel low-cost adsorbent, cellulose-clay composite: Insights from isotherm, kinetic, thermodynamic, and molecular dynamics simulation studies. J Mol Struct. 2023;1291:135865.
[48] Gao Z, Ma D, Chen Y, Zheng C, Teng J. Study for the effect of temperature on methane desorption based on thermodynamics and kinetics. ACS Omega. 2020;6(1):702–14.
[49] Ersoy KK, Orakdogen N. Modulating physico-mechanical, swelling, and adsorption properties of fibrous nanoclay embedded anionically-modified semi-IPNs as new promising materials. Eur Polym J. 2022;167:111084.

[50] Largo F, Haounati R, Akhouairi S, Ouachtak H, El Haouti R, El Guerdaoui A, et al. Adsorptive removal of both cationic and anionic dyes by using sepiolite clay mineral as adsorbent: Experimental and molecular dynamic simulation studies. J Mol Liq. 2020;318:114247.
[51] Saha K, Deka J, Gogoi RK, Datta KKR, Raidongia K. Applications of lamellar membranes reconstructed from clay mineral-based nanosheets: a review. ACS Appl Nano Mater. 2022;5(11):15972–99.
[52] Gul S, Kausar A, Muhammad B, Jabeen S. Technical relevance of epoxy/clay nanocomposite with organically modified montmorillonite: a review. Polym Technol Eng. 2016;55(13):1393–415.
[53] Gabal MA, Al-Zahrani NG, Al Angari YM, Al-Juaid AA, Abdel-Fadeel MA, Alharbi SR, et al. CoFe2O4/MWCNTs nano-composites structural, thermal, magnetic, electrical properties and dye removal capability. Mater Res Express. 2019;6(10):105059.
[54] Al-Saidi HM, Abdel-Fadeel MA, Alharthi SS. Preconcentration and ultrasensitive spectrophotometric estimation of tungsten in soils using polyurethane foam in the presence of rhodamine B: Kinetic and thermodynamic studies, and designing a simple automated preconcentration system. J Saudi Chem Soc. 2021;25(8):101301.
[55] Din SU, Khaqan U, Imran M, Al-Ahmary KM, Alshdoukhi IF, Carabineiro SA, et al. Enhancing arsenic removal using Cu-infused biochar: Unravelling the influence of pH, temperature and kinetics. Chem Eng Res Des. 2024;203:368–77.
[56] Hameed SA, Abdel-Fadeel MA, Al-Saidi HM, Salam MA. Simultaneous removal of the toxic tungsten ions and rhodamine B dye by graphene nanosheets from model and real water. Desalin Water Treat. 2020;188:266–76.
[57] Abdel-Salam M, Al-khateeb LA, Abdel-Fadeel MA. Removal of toxic ammonium ions from water using nanographene sheets. Desalin Water Treat. 2018;129:168–76.
[58] Braun T, Navratil JD, Farag AB. Polyurethane foam sorbents in separation science. Boca Raton: CRC press; 2018.
[59] Hu Q, Lan R, He L, Liu H, Pei X. A critical review of adsorption isotherm models for aqueous contaminants: Curve characteristics, site energy distribution and common controversies. J Environ Manag. 2023;329:117104.
[60] Minju N, Jobin G, Savithri S, Ananthakumar S. Double-silicate derived hybrid foams for high-capacity adsorption of textile dye effluent: statistical optimization and adsorption studies. Langmuir. 2019;35(29):9382–95.
[61] Swenson H, Stadie NP. Langmuir's theory of adsorption: A centennial review. Langmuir. 2019;35(16):5409–26.
[62] Sacco O, Matarangolo M, Vaiano V, Libralato G, Guida M, Lofrano G, et al. Crystal violet and toxicity removal by adsorption and simultaneous photocatalysis in a continuous flow micro-reactor. Sci Total Environ. 2018;644:430–8.
[63] Sidjou AS, Tchakounte AN, Shikuku V, Lenou I, Djimtibaye R, Dika MM. Synthesis of alkali-activated volcanic scoria and rice husk ash based composite materials for adsorptive removal of crystal violet: optimization, kinetics, isotherms and mechanism. Hybrid Adv. 2023;4:100113.
[64] Katowah DF, Abdel-Fadeel MA. Ultrahigh adsorption capacity of a new metal sieve-like structure nanocomposite-based chitosan-graphene oxide nanosheet coated with poly-o-toluidine for the removal of Acid Red dye from the aquatic environment. Nanocomposites. 2023;9(1):80–99.
[65] Akram M, Bhatti HN, Iqbal M, Noreen S, Sadaf S. Biocomposite efficiency for Cr (VI) adsorption: Kinetic, equilibrium and thermodynamics studies. J Environ Chem Eng. 2017;5(1):400–11.
[66] Bhatti HN, Jabeen A, Iqbal M, Noreen S, Naseem Z. Adsorptive behavior of rice bran-based composites for malachite green dye: isotherm, kinetic and thermodynamic studies. J Mol Liq. 2017;237:322–33.
[67] Ewis D, Ba-Abbad MM, Benamor A, El-Naas MH. Adsorption of organic water pollutants by clays and clay minerals composites: A comprehensive review. Appl Clay Sci. 2022;229:106686.
[68] Padil VV, Kumar KA, Murugesan S, Torres-Mendieta R, Wacławek S, Cheong JY, et al. Sustainable and safer nanoclay composites for multifaceted applications. Green Chem. 2022;24(8):3081–114.
[69] Iravani R, An C, Adamian Y, Mohammadi M. A review on the use of nanoclay adsorbents in environmental pollution control. Water Air Soil Pollut. 2022;233(4):109.
[70] Althomali RH, Alamry KA, Hussein MA, Khan A, Al-Juaid SS, Asiri AM. Modification of alginic acid for the removal of dyes from aqueous solutions by solid-phase extraction. Int J Environ Anal Chem. 2022;102(16):3673–93.
[71] Munilakshmi N, Srimurali M, Karthikeyan J. Adsorptive removal of acid red 1, from aqueous solutions by preformed flocs. Int J Curr Eng Technol. 2013;3(4):1456–62.
[72] Salam MA, Gabal MA, Al Angari YM. The recycle of spent Zn–C batteries and the synthesis of magnetic nanocomposite from graphene nanosheets and ferrite and its application for environmental remediation. J Mater Res Technol. 2022;18:4267–76.
[73] Ahmad M, Bachmann RT, Khan MA, Edyvean RG, Farooq U, Athar MM. Dye removal using carbonized biomass, isotherm and kinetic studies. Desalin Water Treat. 2015;53(8):2289–98.
[74] Abd-Elhamid AI, Ali HH, Nayl AA. Modification of sugarcane bagasse as a novel lignocellulosic biomass adsorbent nanocomposite to improve adsorption of methylene blue. Cellulose. 2023;30(8):5239–58.
[75] El Naeem GA, Abd-Elhamid AI, Farahat OO, El-Bardan AA, Soliman HM, Nayl AA. Adsorption of crystal violet and methylene blue dyes using a cellulose-based adsorbent from sugercane bagasse: characterization, kinetic and isotherm studies. J Mater Res Technol. 2022;19:3241–54.
[76] Allangawi A, Aljar MAA, Ayub K, Abd El-Fattah A, Mahmood T. Removal of methylene blue by using sodium alginate-based hydrogel; validation of experimental findings via DFT calculations. J Mol Graph Model. 2023;122:108468.
[77] Rahmi R, Lelifajri L, Fathurrahmi F, Fathana H, Iqhrammullah M. Preparation and characterization of PEGDE-EDTA-modified magnetic chitosan microsphere as an eco-friendly adsorbent for methylene blue removal. South Afr J Chem Eng. 2023;43:296–302.
[78] Handayani T, Ramadhani P, Zein R. Modelling studies of methylene blue dye removal using activated corn husk waste: Isotherm, kinetic and thermodynamic evaluation. South Afr J Chem Eng. 2024;47:15–27.